Supplementary Information: Synthesis, Photophysical Characterization and Integration of Two-Photon Fluorophores in Mesoporous Organosilica Nanoparticles for Biological Imaging Use

Nicolas Bondon [a, b, *], Nicolas Richy [b], Lamiaa M. Ali [c, d], Denis Durand [c], Magali Gary-Bobo [c], Yann Molard [b], Grégory Taupier [b], Frédéric Paul [b], Nadir Bettache [c], Jean-Olivier Durand [a], Christophe Nguyen [c], Clarence Charnay [a, *] and Olivier Mongin [b, *]

1.1 ^{1}H NMR of newly synthesized compounds

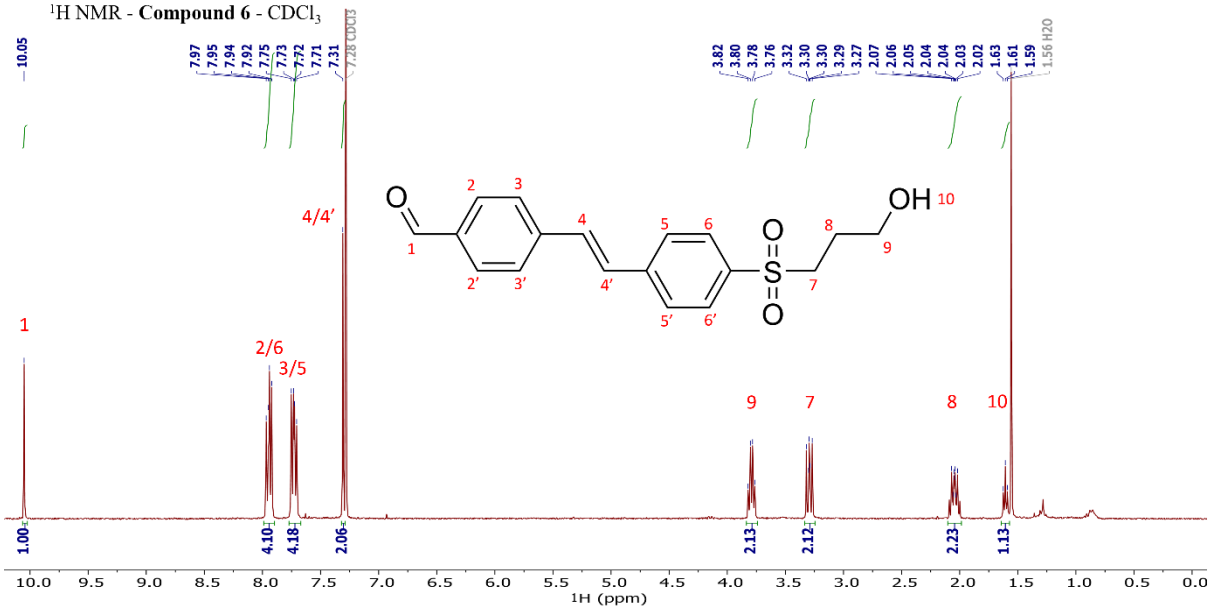

Figure S1. ^{1}H NMR spectrum of intermediate compound **6** (in $CDCl_3$).

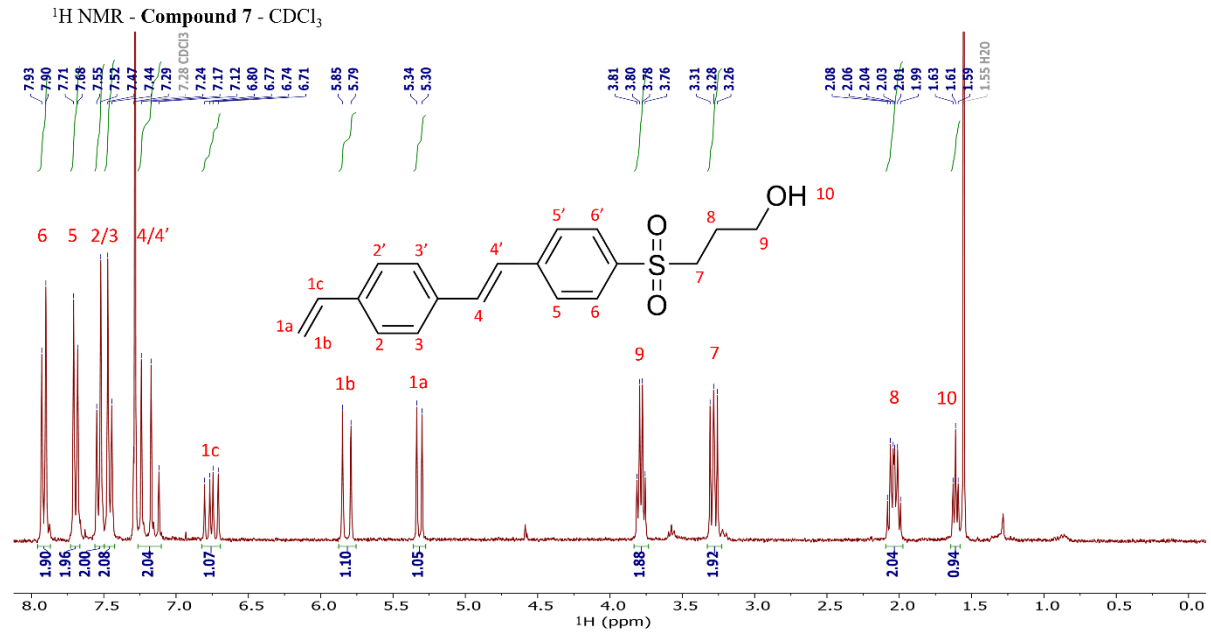

Figure S2. ^{1}H NMR spectrum of intermediate compound **7** (in $CDCl_3$).

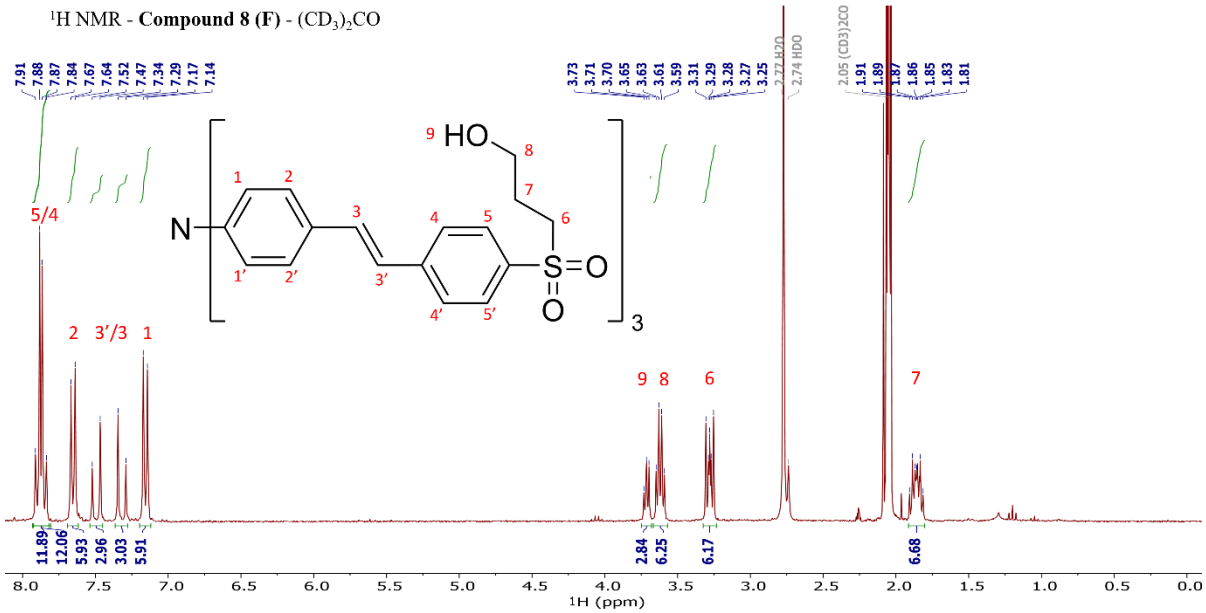

Figure S3. ^{1}H NMR spectrum of **8** (F) bearing one phenylene-vinylene linker (in $(CD_3)_2CO$).

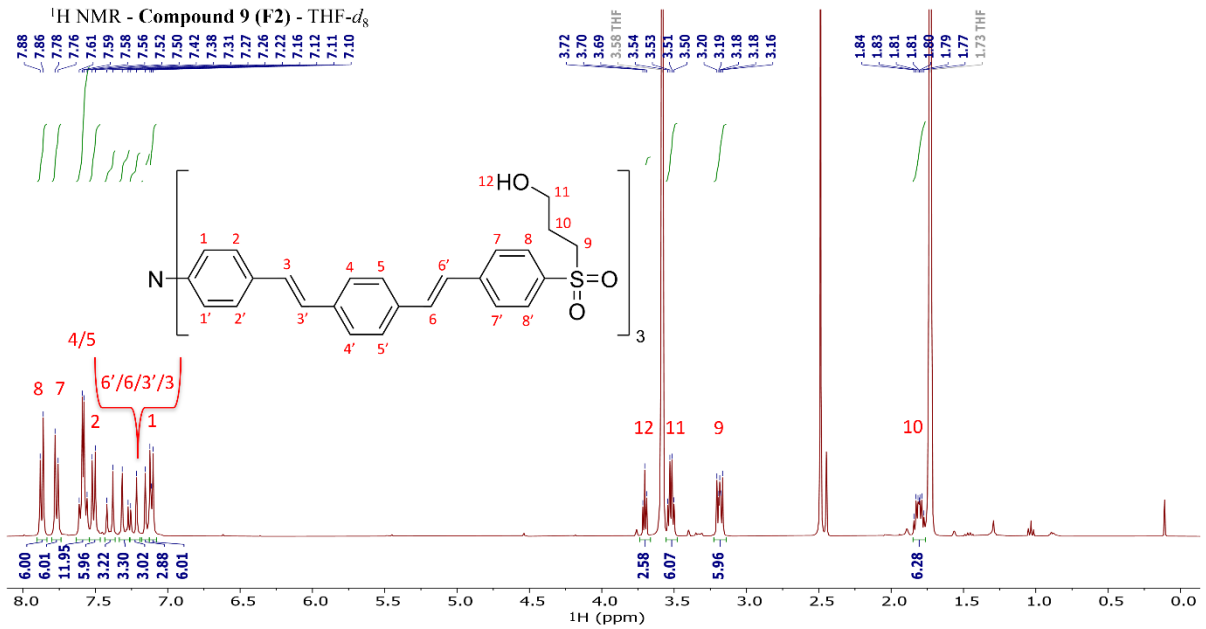

Figure S4. ^{1}H NMR spectrum of three-branched fluorophore **9** (F2) bearing two phenylene-vinylene linkers (in THF-d_8).

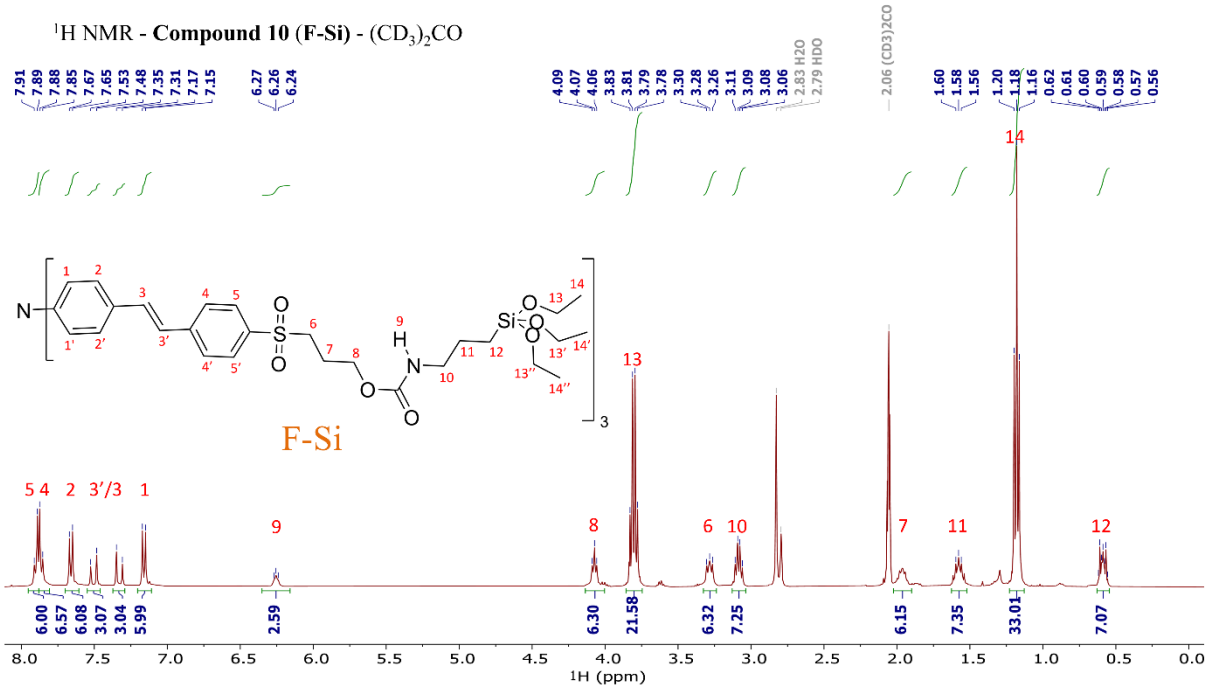

Figure S5. ^{1}H NMR spectrum of the silylated fluorophore **10** (F-Si, in $(CD_3)_2CO$).

1.2 ^{13}C NMR spectra of newly synthesized compounds

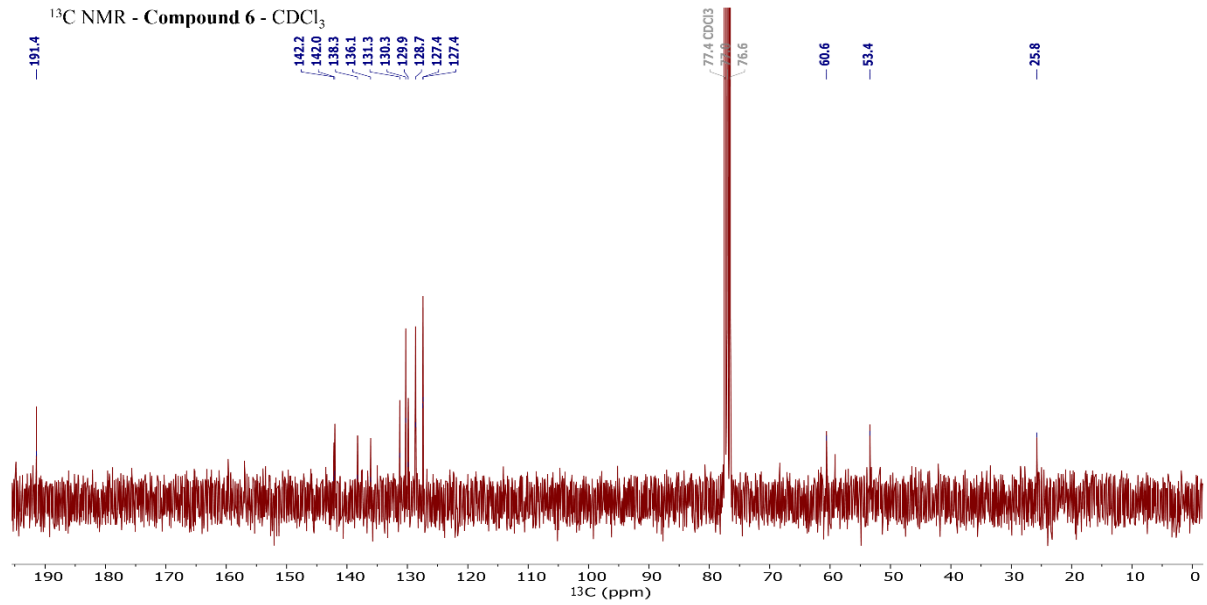

Figure S6. ^{13}C NMR spectrum of intermediate compound **6** (in $CDCl_3$).

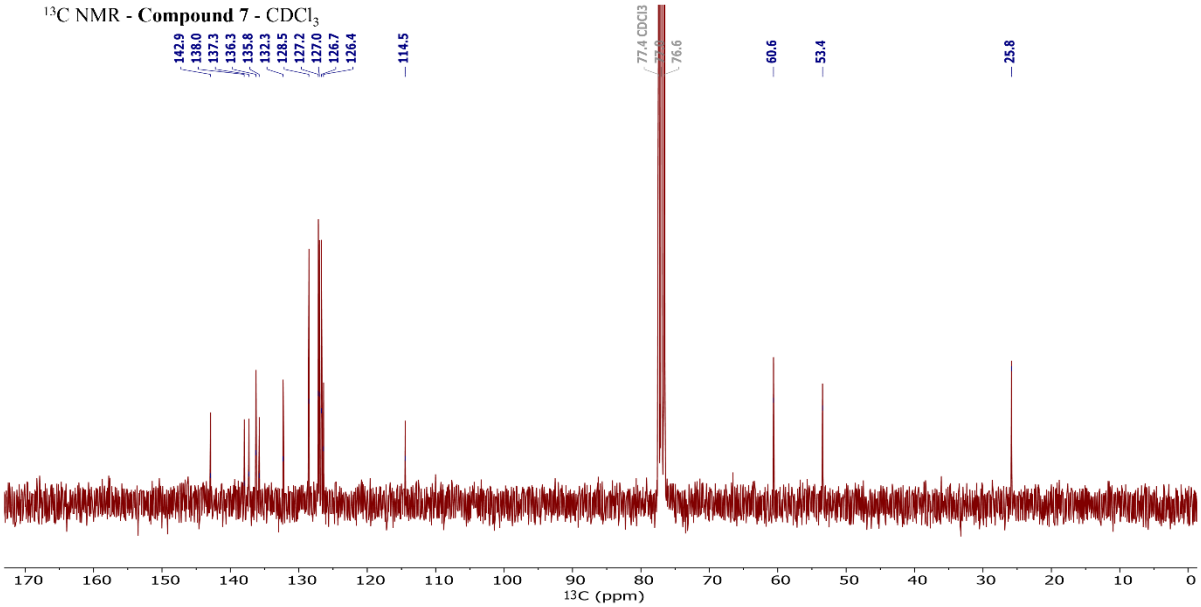

Figure S7. ^{13}C NMR spectrum of intermediate compound **7** (in $CDCl_3$).

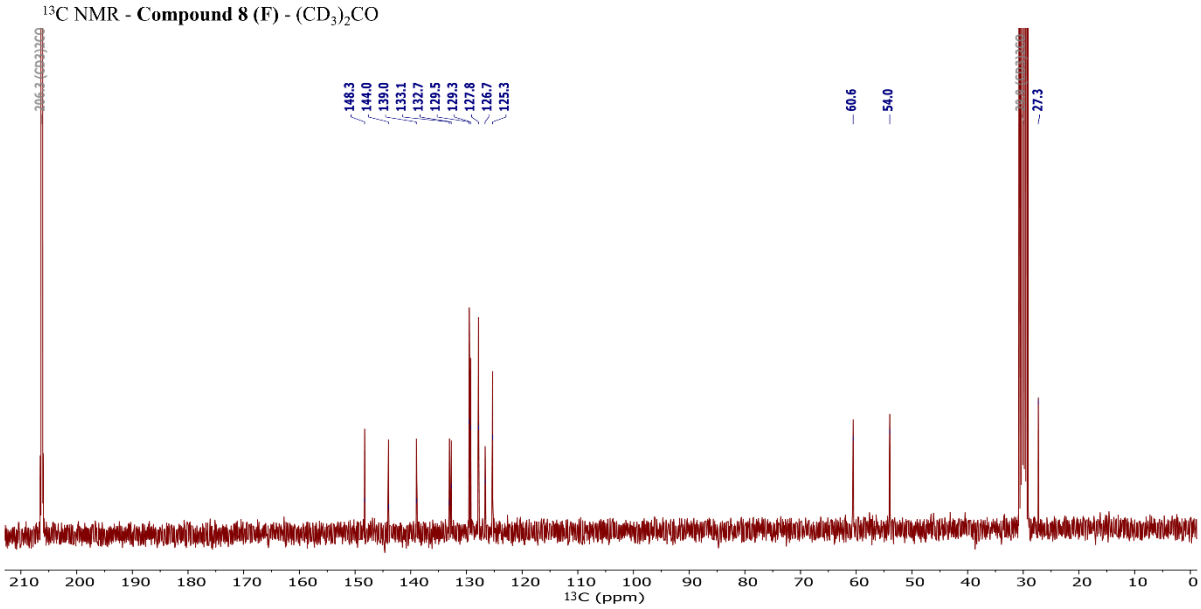

Figure S8. ^{13}C NMR spectrum of **8** (F) bearing one phenylene-vinylene linker (in $(CD_3)_2CO$).

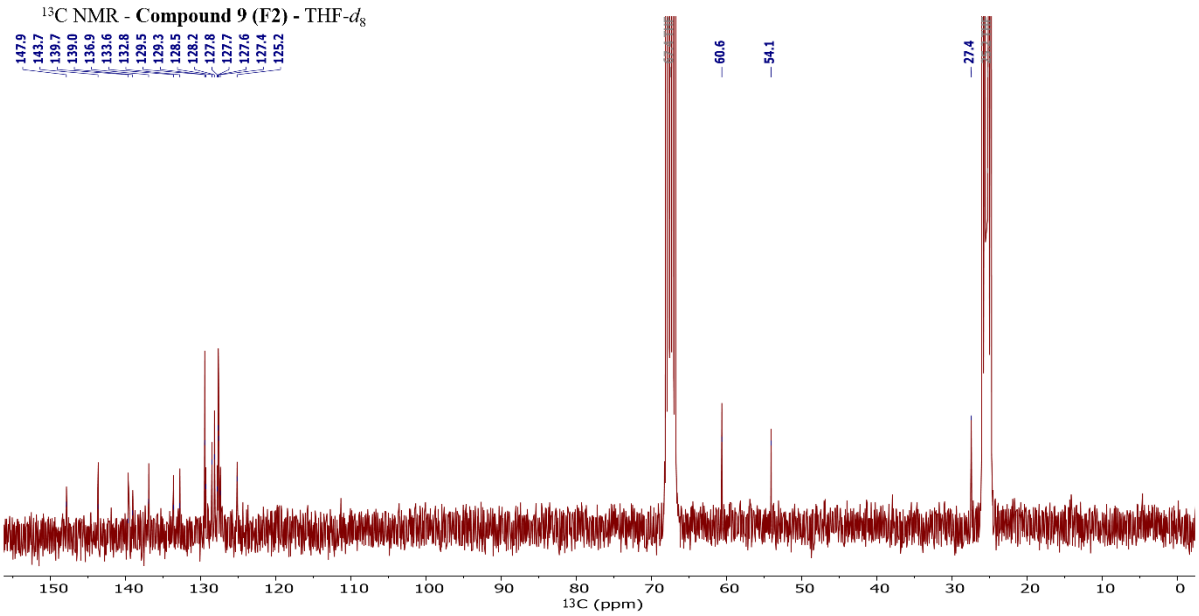

Figure S9. ^{13}C NMR spectrum of three-branched fluorophore **9** (F2) bearing two phenylene-vinylene linkers (in THF-d_8).

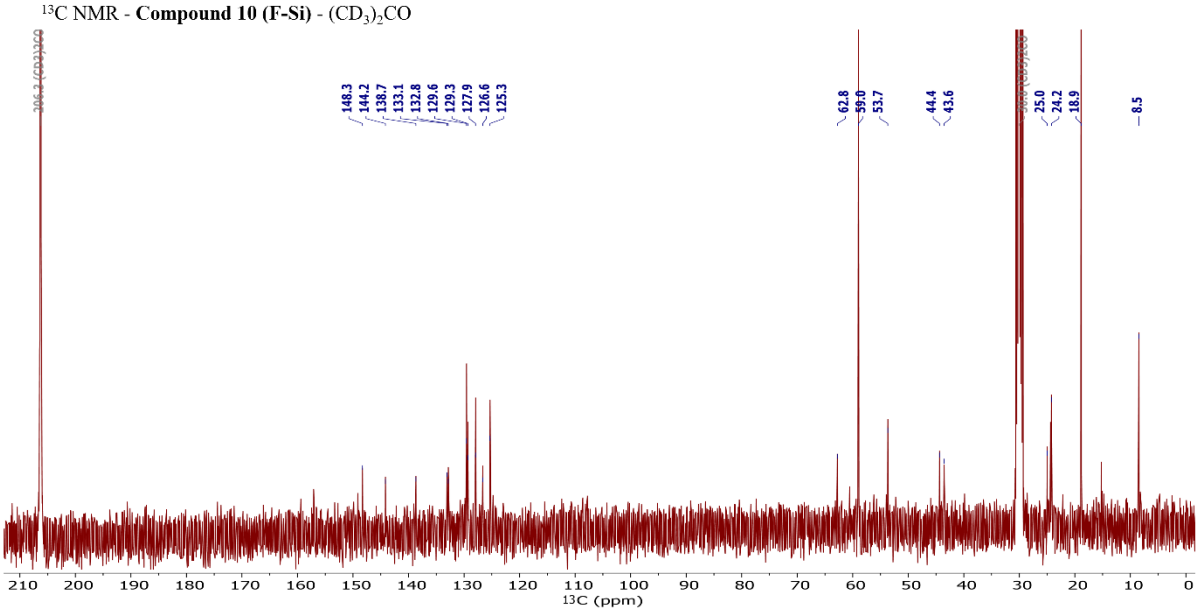

Figure S10. ^{13}C NMR spectrum of the silylated fluorophore **10** (F-Si, in $(CD_3)_2CO$).

1.3 HRMS spectra of newly synthesized compounds

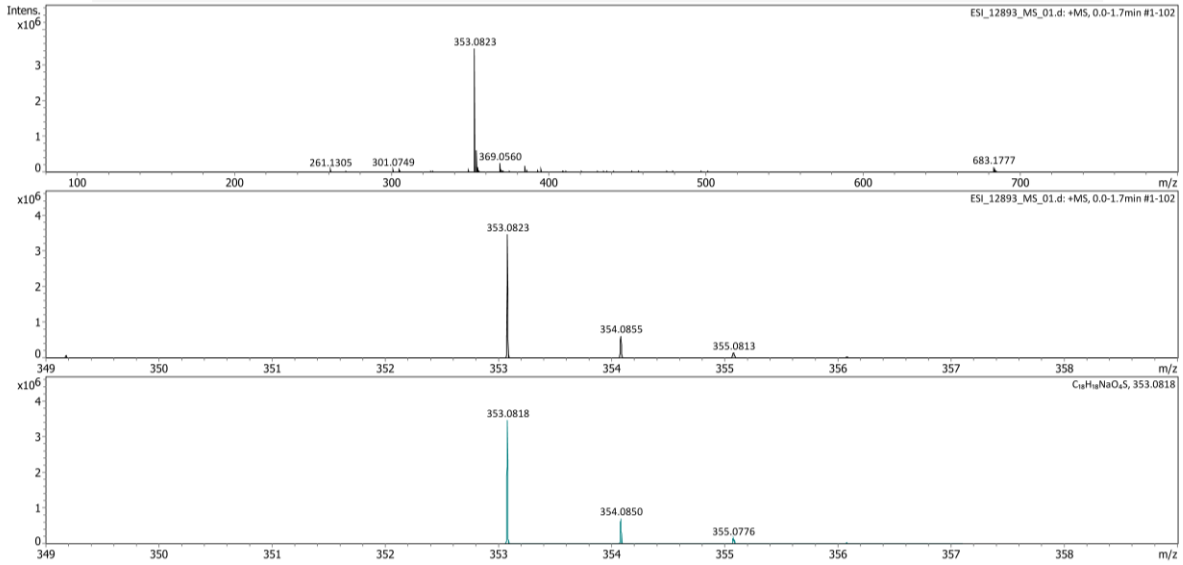

Figure S11. HRMS spectrum (ES^+) of intermediate compound **6**.

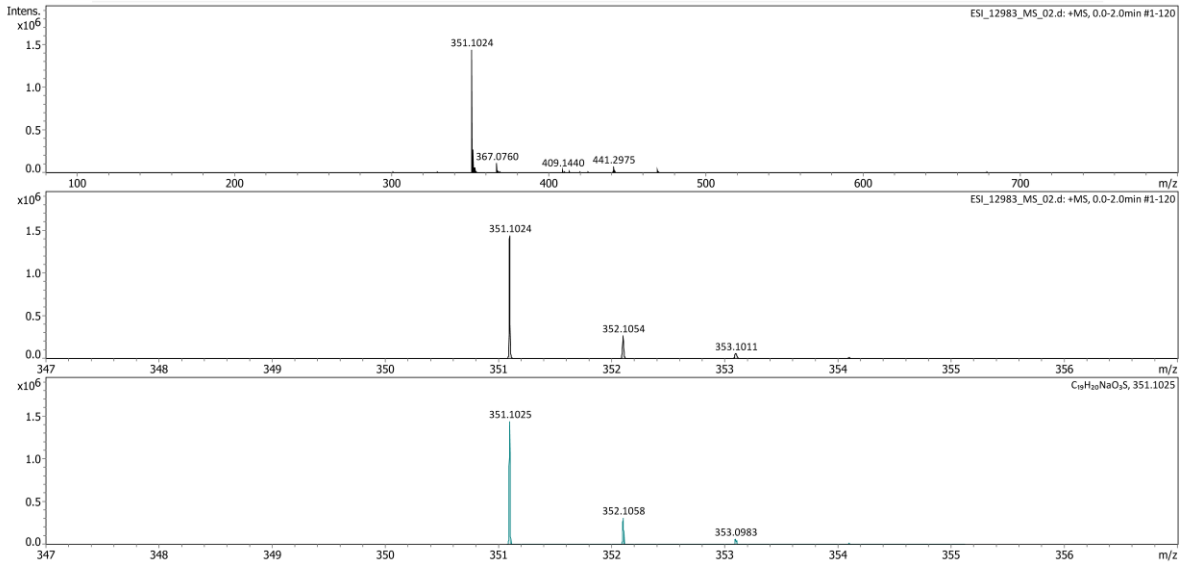

Figure S12. HRMS spectrum (ES^+) of intermediate compound **7**.

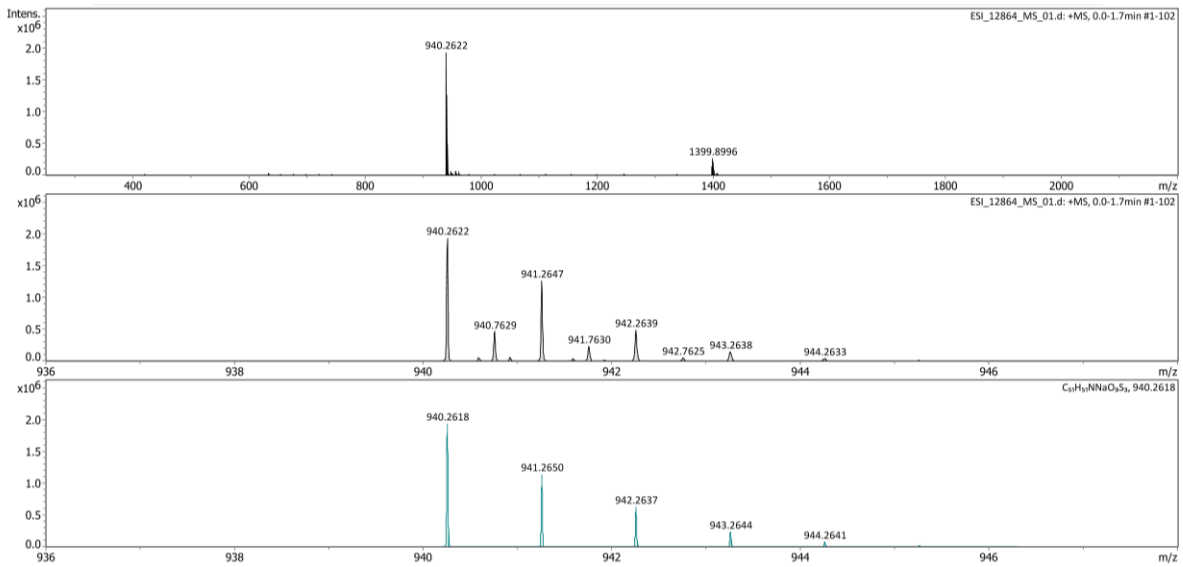

Figure S13. HRMS spectrum (ES^+) of **8** (F) bearing one phenylene-vinylene linker.

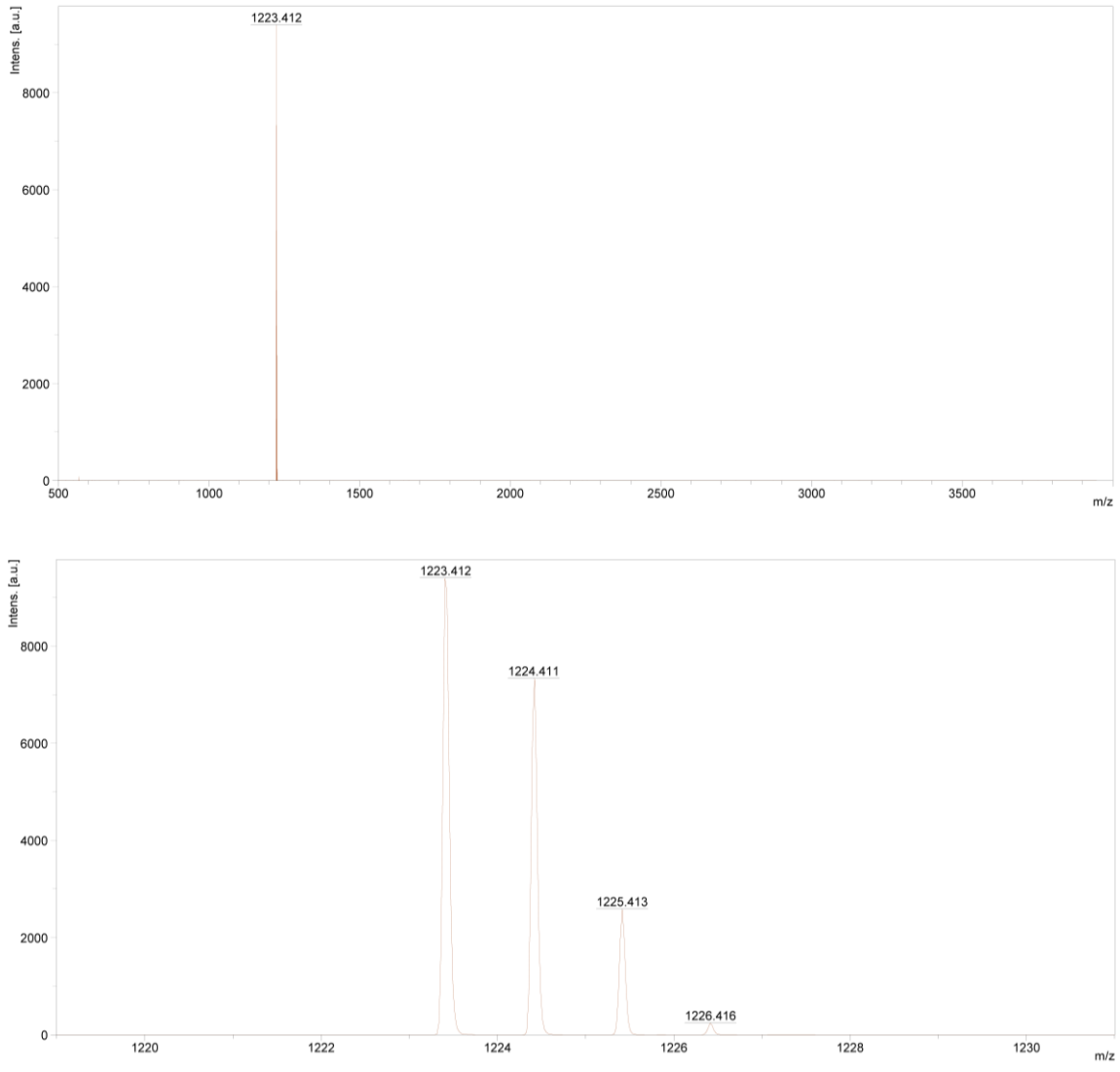

Figure S14. HRMS spectrum (MALDI) of three-branched fluorophore **9** (F2) bearing two phenylene-vinylene linkers.

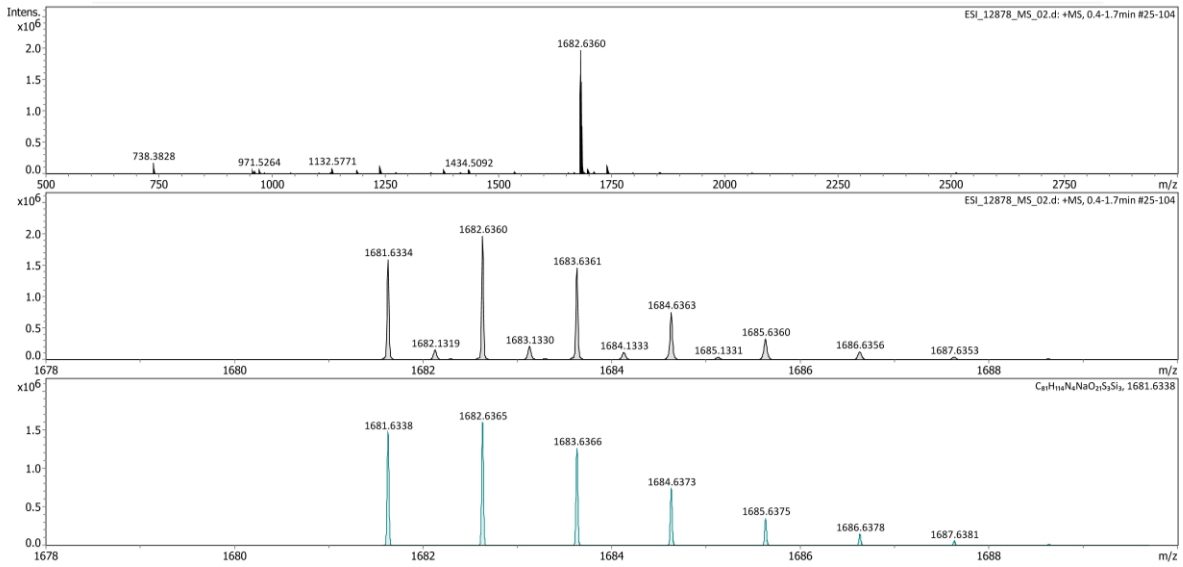

Figure S15. HRMS spectrum (ES^+) of the silylated fluorophore **10** (F-Si).

1.4 Two-photon responsive character of newly synthesized fluorophores

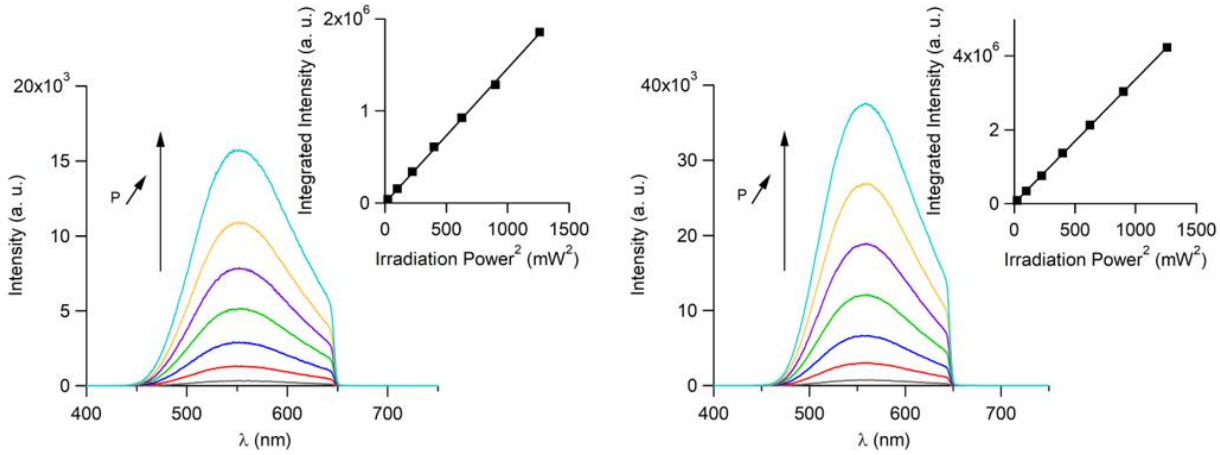

Figure S16. Quadratic dependence of the chromophore's emission intensity on the laser excitation power. Fluorophore F (left) and fluorophore F2 (right) were excited in THF at 700 nm.

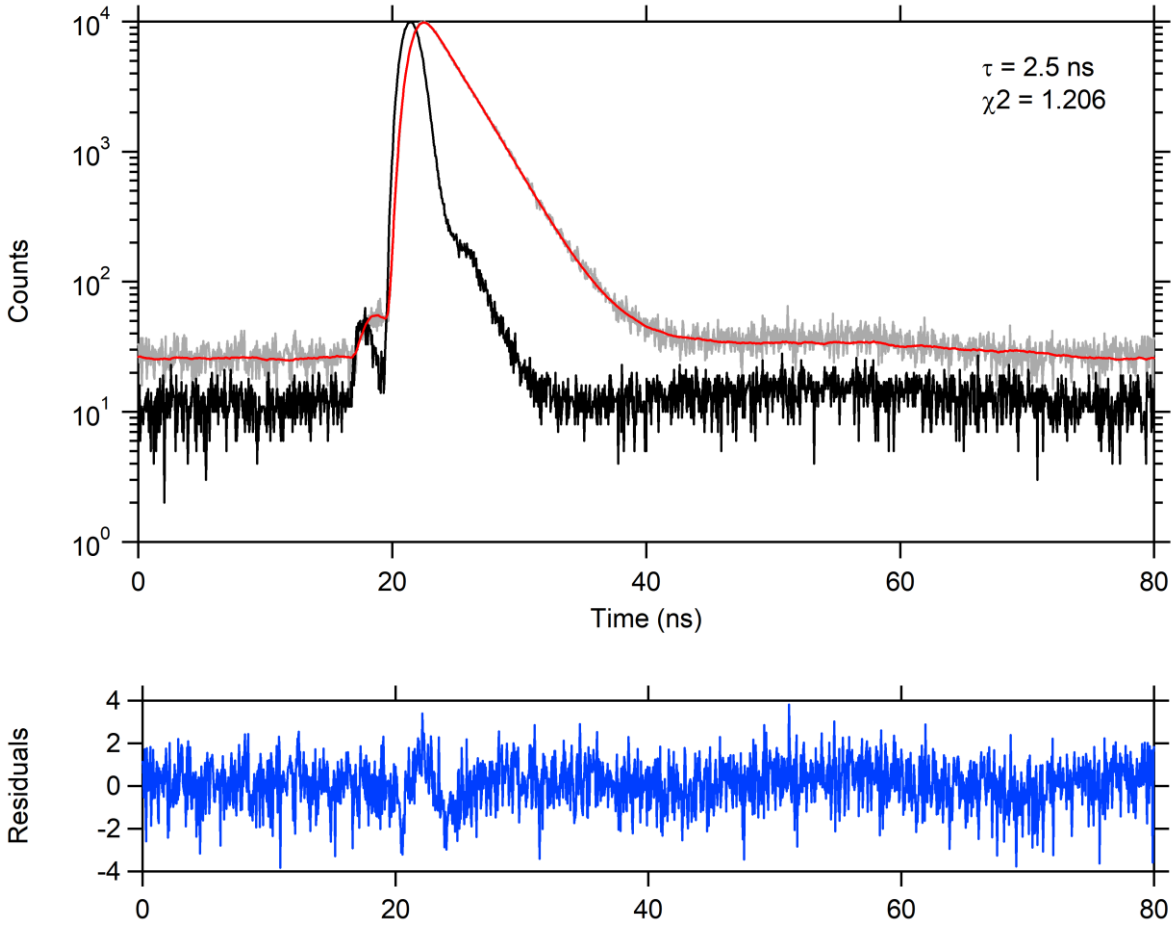

Figure S17. TCSPC data of F in THF (grey curve: measured decay; black curve: IRF; red curve: fitted decay; blue curve: residuals).

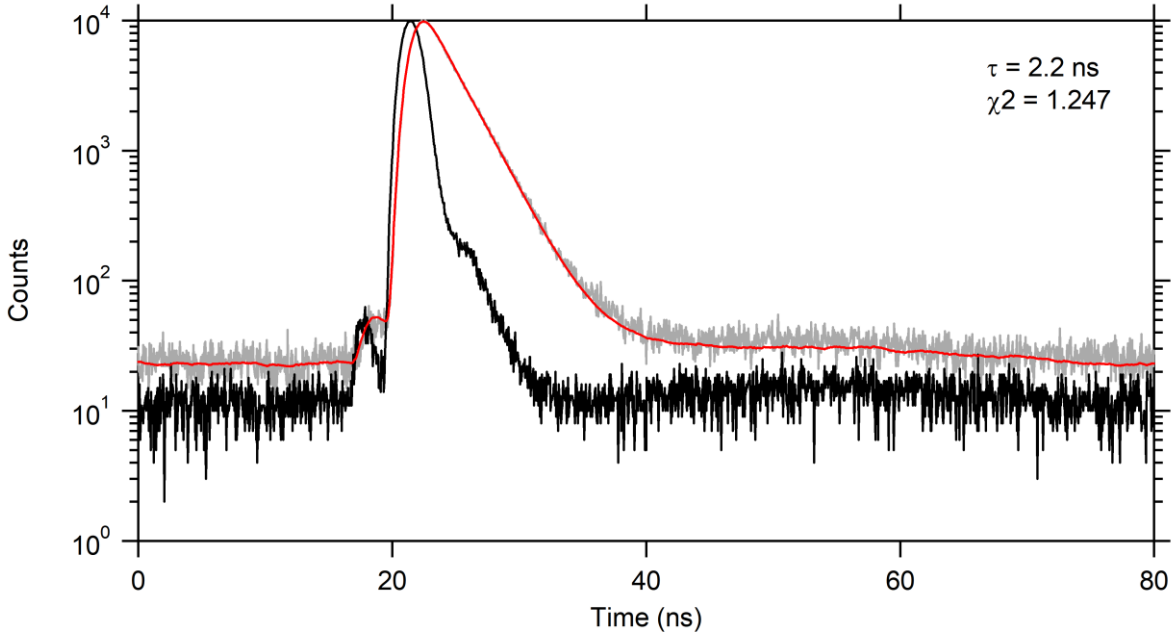

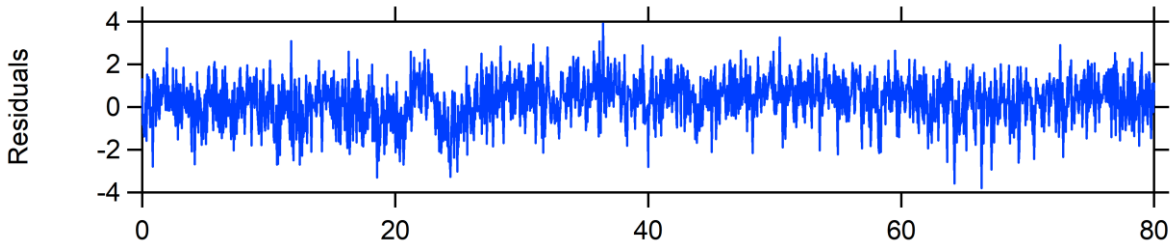

Figure S18. TCSPC data of F2 in THF (grey curve: measured decay; black curve: IRF; red curve: fitted decay; blue curve: residuals).

1.5 Cytotoxicity of fluorophore-based periodic mesoporous organosilica nanoparticles

The cytotoxic effect of the three NPs was studied by incubating MCF-7 cells with increasing concentrations (from 5 to 200 µg mL^{-1}) of NPs for 72 h. Figure S6 shows a very low decrease in cell viability with 76% of viability for E 4S F-2 NPs at the highest concentration and more than 85% for E 4S F-1a and E 4S F-1b NP. These data suggest the biocompatibility of these NPs.

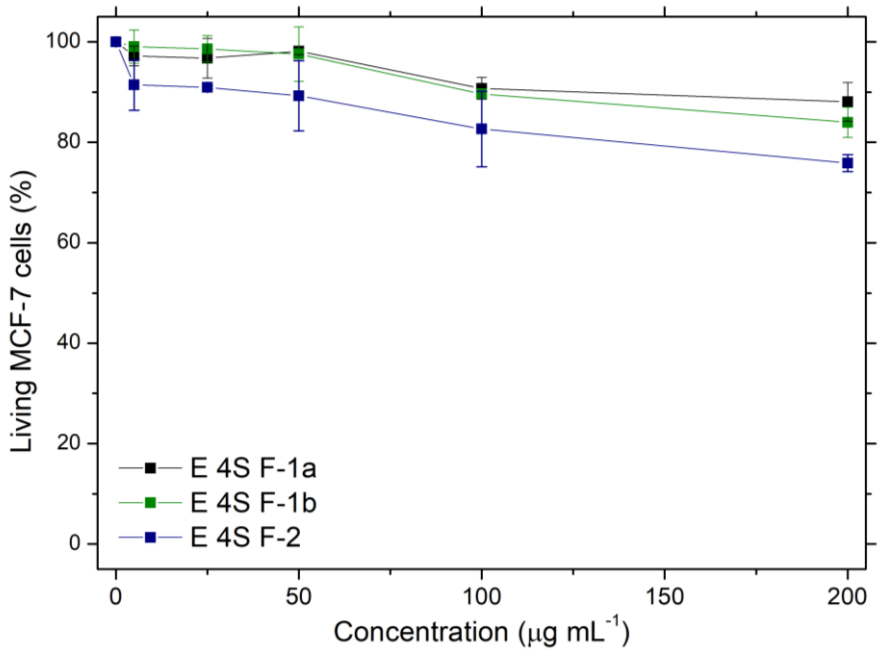

Figure S19. Toxicity studies of different F PMO on human breast MCF-7 cancer cells incubated with different concentrations for 72 h. Data are presented as mean ± standard error of mean (SEM) of two independent experiments.

1.6 Quantification of nanoparticles' internalization in cancer cells from their intrinsic fluorescence

The quantification of fluorophore-PMO NPs inside cancer cells demonstrated that E 4S F-2 is around two-fold more efficiently internalized than E 4S F-1b and four-fold more than E 4S F-1a.

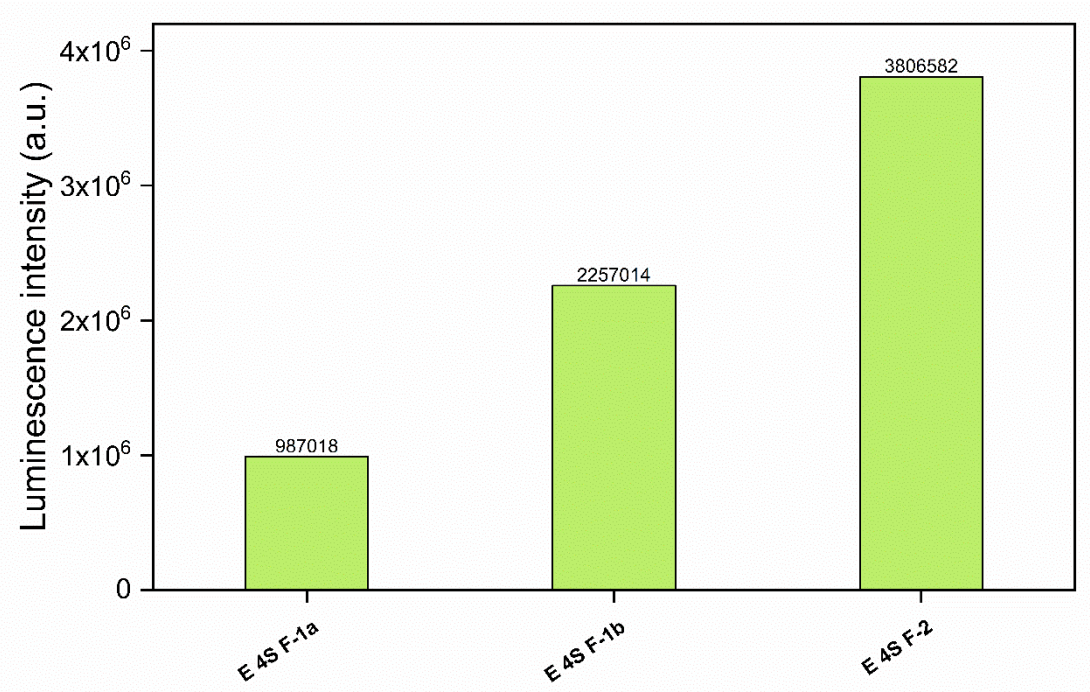

Figure S20. Quantification of fluorophore-PMO NPs inside MCF-7 cells. All the surface of the picture was submitted to quantification using ImageJ software. Values are levels of NP luminescence presented in arbitrary units.